SCIENTIFIC REPORTS

OPEN

SUBJECT AREAS:
TOPOLOGICAL INSULATORS
ELECTRONIC STRUCTURE

Received
18 August 2014

Accepted
14 January 2015

Published
12 February 2015

Correspondence and requests for materials should be addressed to S.-H.J. (jhish@postech.ac.kr)

Quantum anomalous Hall and quantum spin-Hall phases in flattened Bi and Sb bilayers

Kyung-Hwan Jin & Seung-Hoon Jhi

Department of Physics, Pohang University of Science and Technology, Pohang 790-784, Republic of Korea.

Discovery of two-dimensional topological insulator such as Bi bilayer initiates challenges in exploring exotic quantum states in low dimensions. We demonstrate a promising way to realize the Kane-Mele-type quantum spin Hall (QSH) phase and the quantum anomalous Hall (QAH) phase in chemically-modified Bi and Sb bilayers using first-principles calculations. We show that single Bi and Sb bilayers exhibit topological phase transitions from the band-inverted QSH phase or the normal insulator phase to Kane-Mele-type QSH phase upon chemical functionalization. We also predict that the QAH effect can be induced in Bi or Sb bilayers upon nitrogen deposition as checked from calculated Berry curvature and the Chern number. We explicitly demonstrate the spin-chiral edge states to appear in nitrogenated Bi-bilayer nanoribbons.

Manipulation of the electronic band structure and their topological invariants is a key in designing topological materials with tailor-made properties. Controlling the chemical bonding at atomic levels to induce the band inversion[1–2] via the spin-orbit coupling (SOC)[3–7] is a straightforward way to change the topologically-invariant Z_2 number[8–9]. Two-dimensional (2D) materials are advantageous in this respect as their bonding character is relatively easy to modify in post synthesis processes, for example, by surface adsorption. In particular, 2D materials should satisfy two essential requirements to have non-trivial topological phases, the lattice symmetry and large SOC. The first condition was demonstrated in a single-band model of the hexagonal lattice for graphene. Semi-metallic graphene becomes a 2D topological insulator when the SOC opens a gap in the Dirac cones[10–11], known as the Kane-Mele-type quantum spin-Hall (QSH) phase. However, the SOC gap in graphene is too small to exceed the thermal energy[12–15], which blocks the observation of graphene TI phase. Several theoretical models have been proposed to extrinsically enhance the SOC of graphene by direct deposition of hydrogen[16] or heavy element adatoms[17], or by contact to 3D TIs[18]. The second condition of strong SOC may be sufficed by heavy elements such as bismuth, which drives topologically non-trivial electronic states in many 3D TIs[6–7]. Interestingly, the bilayer (or buckled monolayer) structure of Bi has the hexagonal lattice and becomes a two-dimensional (2D) TI[19–21], which has been experimentally synthesized and characterized[22–24].

One intriguing issue is a possibility of utilizing Bi bilayer as a platform to realize the quantum anomalous Hall (QAH) effect in 2D. There has been intense interest to find materials exhibiting the QAH[25–26] effect that needs both internal ferromagnetic ordering and strong SOC. Mercury-based quantum wells[27], graphene[28], silicene[29] and doped TIs[30] are proposed to realize the QAH effect, but difficulty in controlling magnetization and the SOC strength limits the size of the QAH gap to a few meV. We note that the staggered structure of bilayer prone to chemical modification may exhibit variation in topological phases. For example, graphene upon hydrogenation turns into the insulating phase with a staggered hexagonal lattice[31–32]. Other group IV elements in hydrogenated 2D structures are also proposed to induce the TI phase[33]. This feature of hexagonal lattices opens interesting possibility of engineering various topological phases in 2D bilayers via chemical treatments.

In this paper, we report a promising way to realize the large-band-gap Kane-Mele-type QSH and the QAH phases in chemically-modified Bi and Sb bilayers using first-principles calculations. We particularly study the behavior of the Dirac cone and the gap opening in Bi and Sb bilayers upon chemical functionalization or changes in the spin-orbit interaction strength. More interestingly, we explore atomic nitrogen deposition that may produce net magnetic moments as a means of realizing the QAH phase in Bi or Sb bilayers.

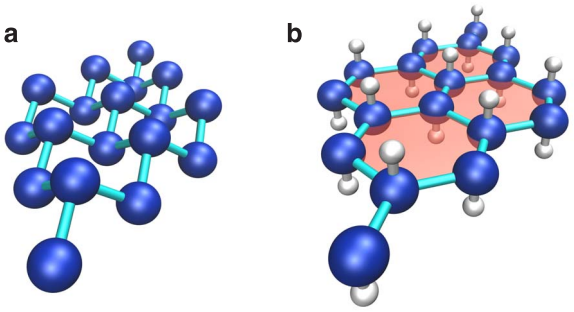

Figure 1 | The lattice geometry for Bi and Sb based structure. Atomic structure of two-dimensional single Bi (111) and Sb (111) bilayers (a) without and (b) with adatom deposition. Blue balls denote Bi or Sb, and white balls the chemicals (H, F or N).

Table 1 | Calculated lattice constants, bond length (between bilayer and decorating atoms), band gap (E_g), SOC gap (Δ_{so}) at K(K') point, and the formation energy (E_f) for hydrogenation (H) or fluorination (F) of Bi and Sb defined as $E_F = E_D - (E_P + E_M)$, where E_D, E_P, and E_M are the total energies of decorated bilayer, the pristine bilayer, and H_2 (or F_2), respectively. The band gap is direct (*d*) for Bi and indirect (*i*) for Sb as indicated in the superscript. Calculated formation-energy favors fluorination over hydrogenation

		Lattice (Å)	Bond length (Å)	E_g (eV)	Δ_{so} (eV)	E_f (eV)
Bi	H	5.50	1.83	1.00^d	1.25	0.24
	F	5.32	2.11	1.02^d	1.14	−1.28
Sb	H	5.28	1.73	0.41^i	0.41	0.18
	F	5.13	1.98	0.33^i	0.33	−1.33

Results

Figures 1 (a) and (b) show the atomic structure of two-dimensional Bi (111) or Sb (111) bilayer and atomically decorated structures (hydrogenated bilayer of Bi and Sb is designated as bismuthane and antimonane, respectively). The buckled configuration is stabilized by both σ and π bonding between Bi (Sb) atoms. Deposition of atomic hydrogen or fluorine on Bi and Sb bilayer makes a flat geometry the same as graphene when the decorating atoms saturate π orbitals. Compared to the structure without adatom deposition, the Bi-Bi and Sb-Sb bonds slightly expand to form the flat geometry. We calculated the phononband structure to check the stability of bismuthane and antimonane and found no imaginary frequencies. Also molecular dynamics simulations show that hexagonal bismuthane and antimonane lattices are dynamically stable up to room temperatures (Figures 2). We note that hydrogenation of Bi and Sb bilayers is endothermic whereas fluorination is exothermic (Table 1). The energy barrier for the hydrogenation is calculated to be about ~3.2 eV. For comparison, the H_2 dissociative reaction barrier in graphene is reported to be 2.7~3.3 eV[34–35]. As hydrogenated graphene is successfully synthesized, the hydrogenation of Bi bilayer is also expected to be feasible at moderate conditions.

Figure 3 shows calculated band structures of bismuthane and antimonane. Without the SOC, we observe exactly the same feature of linear-band Dirac cones as in graphene at K (also K') point. Without the SOC, the Dirac cones at K and K' points in bismuthane (antimonane) are anisotropic with the Fermi velocity of 0.87 × 10^6 m/s (0.85 × 10^6 m/s) along the K-M direction and 0.81 × 10^6 m/s (0.77 × 10^6 m/s) along the K-Γ direction. When the SOC

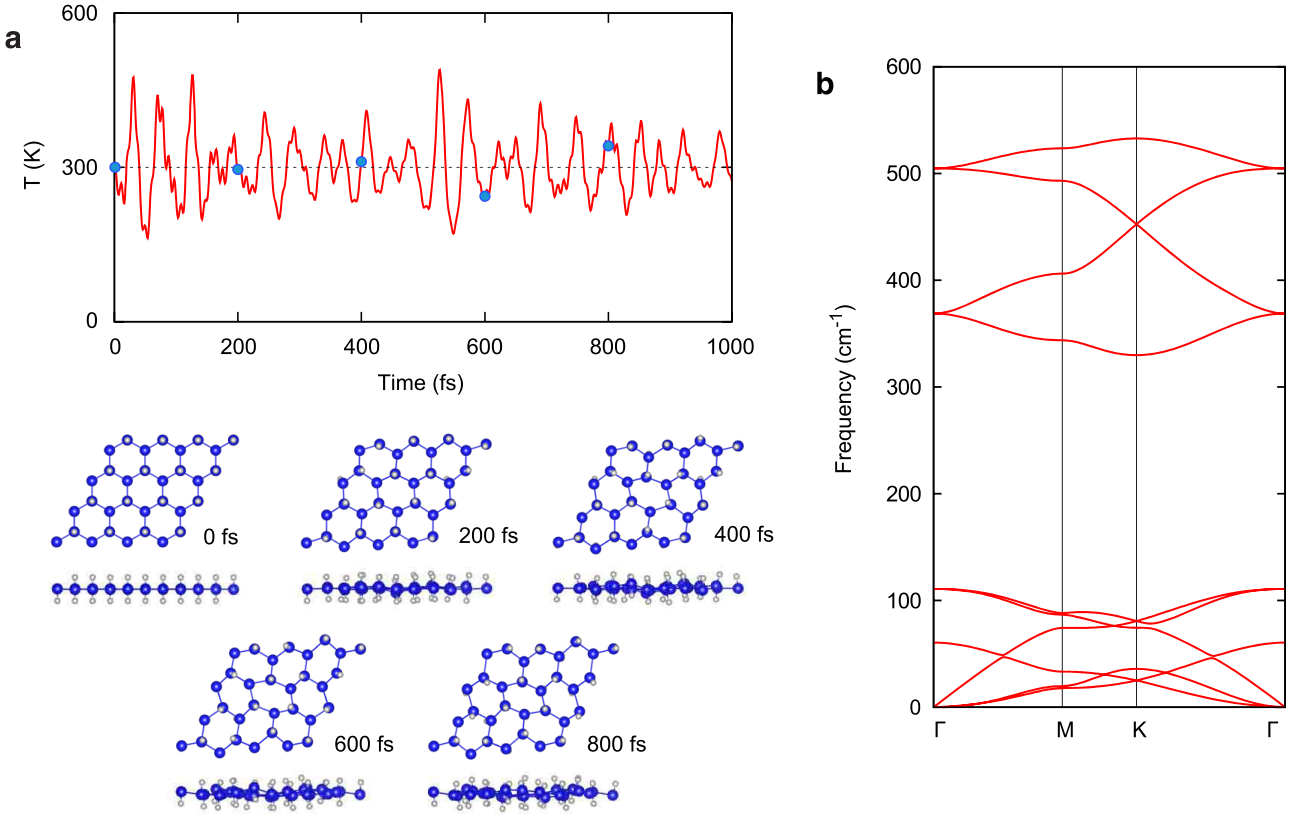

Figure 2 | Structural stability of bismuthane: MD simulation and phonon spectrum. (a) Molecular dynamics (MD) simulation using the NVT ensemble for a 3 × 3 bismuthane at 300K; (upper panel) the temperature variation in time with blue dots denoting the time steps at which the snap shots (lower panel) are taken. Atomic deformation is insignificant, supporting the structural stability at room temperature. (b) Calculated phonon band structure without the SOC for bismuthane. No imaginary frequency is observed, again supporting the structural stability of bismuthane.

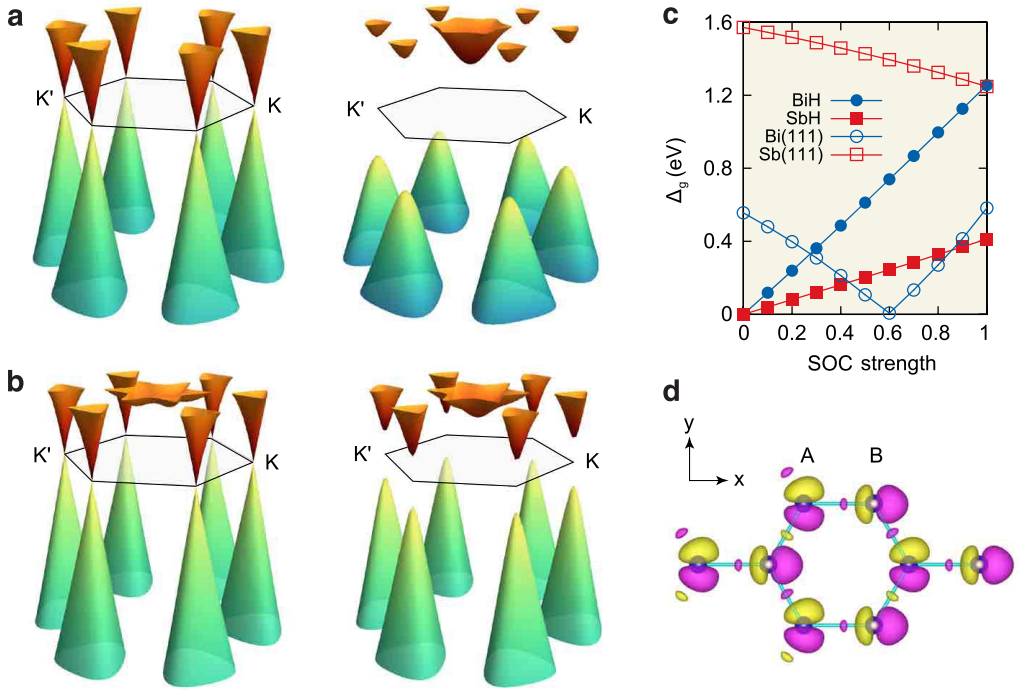

Figure 3 | Electronic properties of chemically modified bilayer system. Calculated Dirac-cone band structures of (a) bismuthane and (b) anitmonane near the Fermi level without SOC (left) and with SOC (right). (c) The energy gaps at Γ or K(K') point for pristine or hydrogenated Bi and Sb (111) bilayers upon varying the spin-orbit coupling strength in first-principles calculations from zero to the true value set as 1. (d) Wannier orbitals constructed from the Dirac states near the Fermi level. Bi p_y (p_x) orbitals represented at A (B) site of the hexagonal lattice. The sign of the wave function is represented in purple (+) or yellow (−) color.

is turned on, bismuthane and antimonane have band gaps at K (K') point of about 1.25 and 0.41 eV, respectively, to become 2D topological insulators of a type proposed by Kane and Mele. The SOC gap of bismuthane and antimonane is proportional to the atomic SOC strength (~1.2 and 0.4 eV[36] for Bi 6*p* and Sb 5*p*, respectively). Similar results are also reported in a recent arXiv paper[37]. The spin-Hall phase of the Kane-Mele type in bismuthane and antimonane is directly checked from the behavior of the SOC gap upon changing the SOC strength in our first-principles calculations. The linear relation of the gap to the SOC strength in Fig. 3 (c) is a clear sign of the Kane-Mele type QSH phase compared to the case of the band-inversion type QSH phase, which should undergo the gap-closing at a certain SOC strength (the transition from band insulator to topological insulator).

The topological transitions induced by hydrogenation (or fluorination) occur in different manners for Bi and Sb bilayers. We note that the Bi (111) bilayer is a 2D topological insulator whereas the Sb (111) bilayer is a normal insulator (Supplementary Information 1). In addition, the Bi (111) bilayer and bismuthane belong to different classes of 2D topological insulators. The Bi (111) bilayer is a topological insulator induced by the band inversion between $p_{x,y}$ and p_z bands at Γ point. On the other hand, bismuthane, which has Dirac cones at K(K') point by the hexagonal lattice symmetry in the absence of the SOC, turns into a topological insulator when the SOC opens a gap at the Dirac cones. The Dirac state is mostly composed of p_x and p_y orbitals from Bi atoms as analyzed by maximally localized Wannier functions. [Fig. 3(d)] For Sb (111) bilayer, the atomic SOC of Sb (~0.4 eV) is not strong enough to cause the band inversion to induce the topological phase. Hydrogenation, on the other hand, flattens the Sb (111) bilayer into a hexagonal lattice, which enforces the Dirac cones to form in the absence of the SOC. Indeed, a gap should open due to the SOC at the Dirac point of antimonane regardless of its strength. This is a similar case to graphene when the SOC is considered and we can understand using a simplest four-band model with p_x and p_y orbitals (Supplementary Information 2). Fluorination also induces the same type of the QSH phases for Bi and Sb bilayers (Supplementary Information 3).

One essential characteristic of 2D topological insulators is the existence of helical edge states. To explicitly demonstrate the QSH phase of bismuthane and antibmonane, we constructed their nanoribbon structures and calculated the edge states. Similar to graphene, various types of edge-atomic structures are possible and we considered the zigzag-type and armchair-type edges with or without edge-passivation by hydrogen. Figure 4 shows calculated band structures with the SOC strength artificially set to partial fractions of the true value to check the evolution of the edge states. When the SOC is turned off, three spin configurations in the edges are available in the zigzag-edge nanoribbons exactly the same as in graphene nanoribbons; parallel spin orientation (ferromagnetic), antiparallel spin orientation (antiferromagnetic), and no spin ordering (paramagnetic). Among these, the antiferromagnetic ordering is the most stable according to our calculations. However, when the SOC is turned on and gradually increased to the true value, the magnetic ordering disappears as the bulk gap is opened at K point. Also helical edge states are developed inside the bulk gap with the Dirac point at either the Γ or X point depending on the edge passivation. Without the hydrogen passivation, the Dirac cone is formed at the Γ point, and moves to the X point upon passivation. The position of the Dirac cone is determined by the orbital and bonding characters at the edges. Hydrogen passivation changes the π-bonding at the edges to the *s*-orbital bonding that has an "uphill-shape" band dispersion along Γ-X. This indicates a possibility of the Dirac-cone engineering by chemical passivation[38]. For example, single-edge passivation of Bi nanoribbons will generate one Dirac cone at the Γ point and the other at X point. The edge states at these two Dirac cones cannot interact with each other even at very narrow nanoribbons because

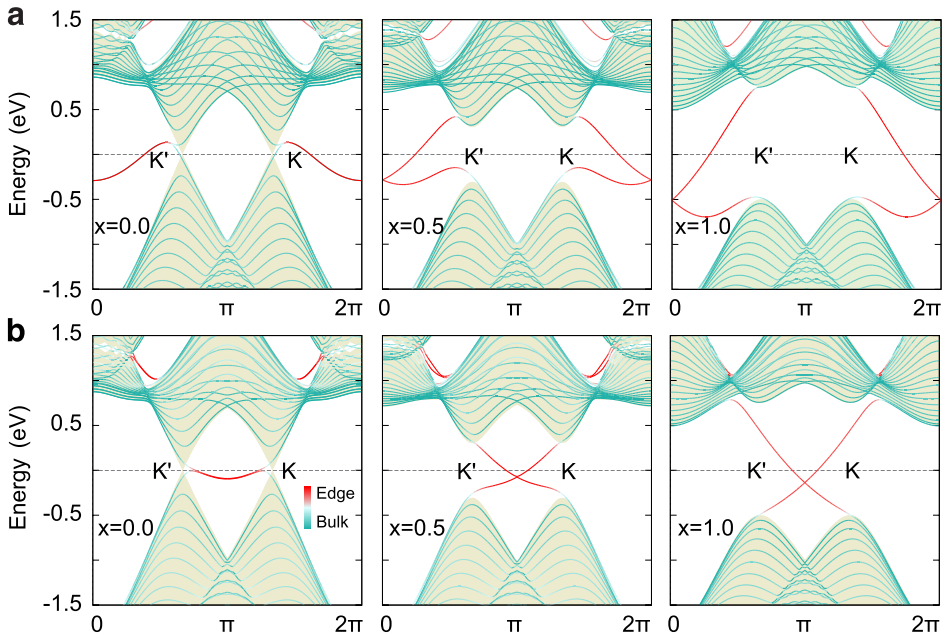

Figure 4 | Edge states of QSH phase Bismuthane. Evolution of the edge states as the SOC strength (x) is changed from 0 to 50 (0.5), and to 100% (1.0) of the true value in bismuthane nanoribbons (a) with the zig-zag edge without passivation and (b) with the hydrogen-passivated zigzag edge. The edge states (depicted in red) have a linear dispersion with the Dirac point at Γ (without passivation) or at X point (hydrogen passivation). The 2D bulk bands projected on the 1D Brillouin zone are depicted in green.

their Bloch wave-vectors are different. The armhair-edged nanoribbons do not exhibit such a feature, having Dirac cones always at the Γ point regardless of passivation (Figure 5).

As nitrogen can have a net magnetic moment upon adsorption on TI surfaces[39], the nitrogen deposition may realize the QAH effect in the Bi bilayer once the magnetic moment of nitrogen is ordered in the ferromagnetic state[30,40]. We tested this possibility in the Bi bilayer. In order to insure the structural stability, we decorated Bi bilayer one side by hydrogen and the opposite side by nitrogen designated as Bi(HN). We checked the structural stability of Bi(HN) from the phonon spectrum and the molecular dynamics simulations. We calculated the phonon frequency of Bi(HN) and found no imaginary frequencies, ensuring the structural stability without any instantaneous bonding distortion. Also molecular dynamics simulations show that Bi(HN) is also dynamically stable up to room temperatures (Supplementary Information 4). The Bi(HN) has a flat 2D structure like bismuthane and possesses a net magnetic moment of $2\mu_B$ per unit cell mostly from N p_x and p_y orbitals (for details of orbital analysis, see the projected density of states in Fig. S5 of Supplementary). The ferromagnetic phase is found to be more stable than the antiferromagnetic state by 5 meV per unit formula in Bi(HN). Calculated band structure of Bi(HN) in Fig. 6(a) shows a split of the spin-up and spin-down bands. To check the topological phase, we calculated the Berry curvature and the Chern number. The non-zero Berry curvature is localized around K' points with the identical sign as shown in Fig. 6(b), and integrating the Berry curvatures over the first Brillouin zone gives the Chern number of 1 for each Dirac cone at K' point, confirming the QAH phase in Bi(HN). A more explicit demonstration of QAH phase is the presence of the chiral states at the edges. Figure 6(c) shows the gapless chiral edge-states inside the bulk gap in Bi(HN) nanoribbons. The number of the edge states should equal the absolute value of the Chern number, and we observe only one chiral edge state in the Dirac gap consistent with calculated Chern number. This is in contrast to the topological insulating phase that has a pair of linear bands with the same helicity at each edge.

A sufficient exchange field is required to realize the QAH phase in Bi and Sb bilayers. As the exchange field depends on the nitrogen coverage, we checked the critical coverage for the QAH phase to emerge in the supercell. Figure 7 shows calculated band structures of the Bi bilayer nitrogenated with increasing coverage (ρ_N) using 2 × 2 supercell. As increasing the nitrogen coverage, the splitting of the spin-up and spin-down bands increases. The band inversion between spin up and down states occurs at about 0.65ML (or 65% adsorption on available sites) of nitrogen coverage, where the QSH phase

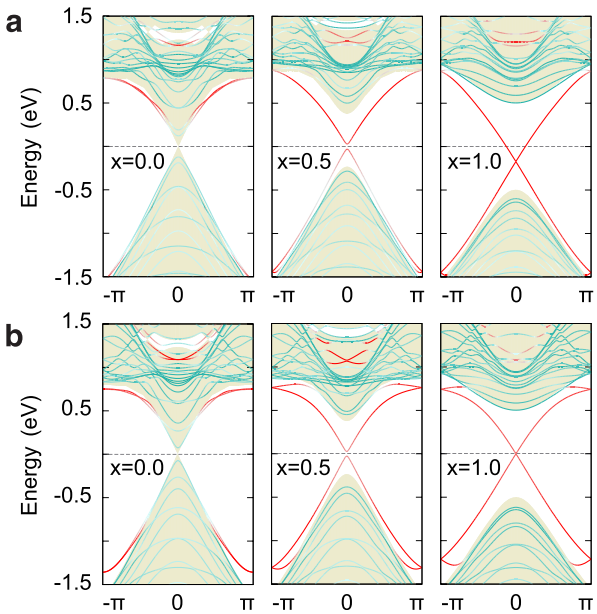

Figure 5 | Edge states of armchair-edged Bismuthane nanoribbons. A similar plot as in Fig. 4 with the SOC strength (x) set to 0, 50 (0.5), and to 100% (1.0) of the true value. The armchair-edged bismuthane nanoribbons have a linear dispersion with the Dirac point at Γ regardless of the edge passivation; (a) no passivation and (b) the hydrogen passivation. The 2D bulk-bands projected on the 1D Brillouin zone are depicted in green.

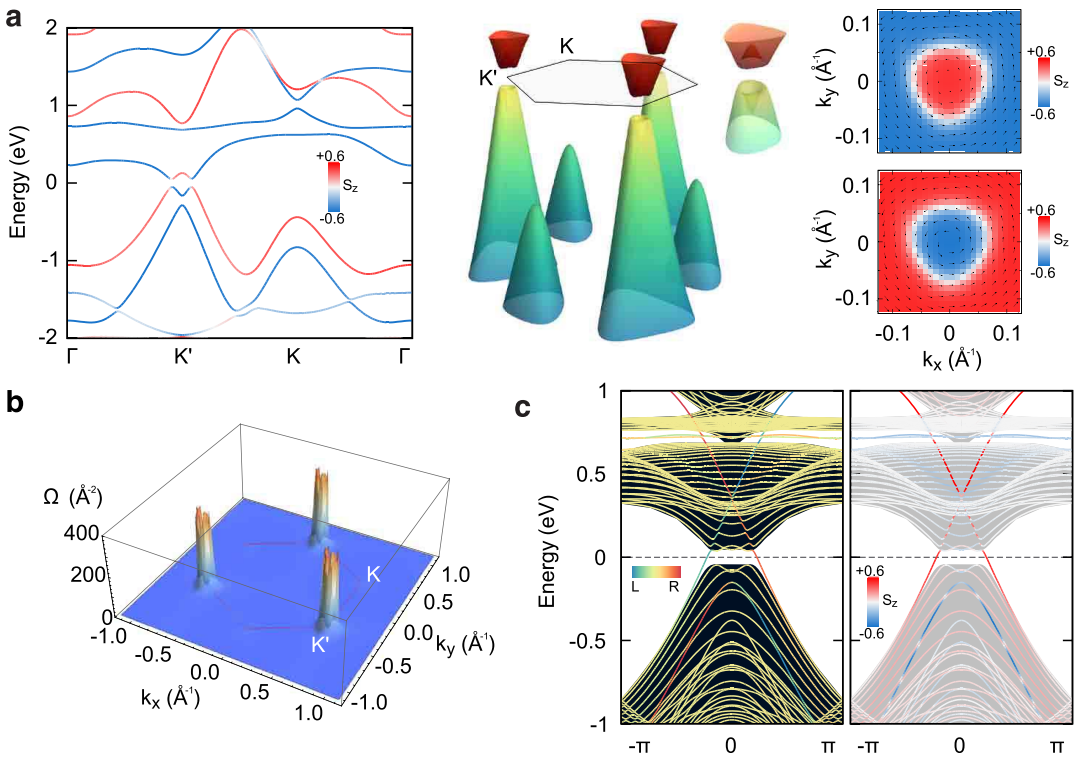

Figure 6 | Realization of QAH phase in Bi bilayer. (a) Calculated band structures of Bi(HN) (left panel). Color (red/blue) of the bands represents the spin (up/down) with detailed spin texture near the Dirac point on the right panel. (b) Calculated Berry curvature of the valence band with the hexagon in red denoting the first Brillouin zone. (c) Calculated edge band-structures of armchair-edged Bi(HN) nanoribbon. The dark region represents the bulk bands projected onto the 1D Brillouin zone of the edges. Left panel shows the site projection to the left (blue) or right (red) edges and right panel the spin z-component with up (red) or down (blue). We observe only one linear band inside the bulk gap with the same spin, which is a direct proof of the quantum anomalous Hall effect.

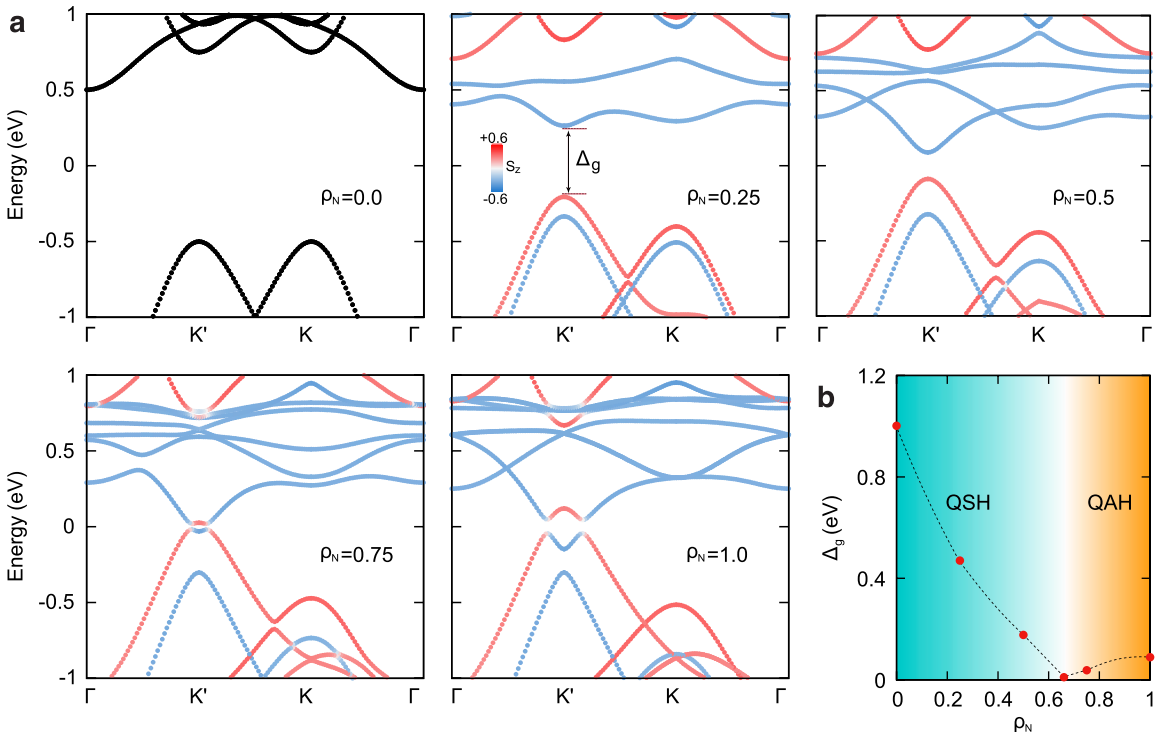

Figure 7 | Nitrogen coverage for the band inversion and QSH-QAH phase transition. (a) Calculated band structures of Bi bilayer nitrogenated with coverage ρ_N using 2×2 supercell. As the nitrogen coverage is increased, the exchange field is enhanced to split the spin up and down states. (b) The band gap as a function of ρ_N. It closes at about 0.65ML where the topological phase transition from QSH to QAH phases occurs.

changes to the QAH phase. The calculated Hall conductance leads to a jump from 0 to 1 at the corresponding critical coverage. Also we calculated nitrogen binding energy on both the edge and bulk of 1.35 and 1.31 eV, respectively. Difference in the binding energy is insignificant, and we expect that nitrogen coverage sufficient for QAH as estimated can be achieved. The binding energy difference of 0.04 eV implies that nitrogen may prefer the edge at low coverages and low temperatures. At moderate temperatures, however, this difference would not block the bulk binding to have nitrogen binding above the critical coverage for the QAH.

Discussion

Chemical modification of low dimensional material is an effective way to alter the electronic properties with desirable features. Our theoretical prediction of large-gap QSH and QAH phases in chemically-modified Bi and Sb bilayers is thus a conceptual proof of such an approach. Practically, synthesis of free-standing bismuthane and antimonane bilayers may not be straightforward, but recent experiment has shown that Bi film can be grown in a very well-ordered manner on TI substrates[22–24]. Utilizing Bi bilayers on substrates and subsequent gas adsorption, for example, we expect that chemically-modified bilayers such as bismuthane and antimonane can be produced.

We showed that the staggered bilayer structure of Bi and Sb experiences intriguing topological phase transitions upon chemical modification such as hydrogenation, fluorination or nitrogenation. We showed that the hydrogenation converts the Bi (Sb) bilayer from the band-inverted QSH phase (normal insulating phase) into Kane-Mele type QSH with a spin-orbit band gap significantly larger than the one in graphene. More interestingly, it was found that the nigrogenated Bi and Sb bilayers have the QAH phase as confirmed by calculated Chern number, and we explicitly demonstrated the chiral edge states in their nano-ribbon structures. Our study reveals intriguing topological properties in the electronic structure of Bi and Sb bilayers upon chemical deposition, which can be utilized for exploring exotic topological phases in low dimensions and for applications of 2D topological insulators.

Methods

First-principles calculations based on the density functional theory were performed using the Vienna ab initio simulation package and the projector-augmented-wave pseudo-potentials in the plane-wave basis with an energy cutoff of 400 eV[41–42]. The exchange-correlation of electrons was treated within the generalized-gradient approximation of Perdew-Burke-Ernzerhof type[43]. The SOC was included in the step of the self-consistent calculations of electronic structure. The k-point meshes of 21 × 21 × 1 were used for the sampling of the Brillouin zone, and the atomic structures were fully relaxed until the Helmann-Feynman forces were less than 0.01 eV/Å. A vacuum region with a thickness of 20 Å or larger was introduced between the bilayers to minimize the artificial interactions in the super-cell method. In order to identify the topological property of the bilayers, the Berry curvature $\Omega(\mathbf{k})$, is calculated using the Kubo formula[44–45]. The Chern number is then evaluated by integrating the Berry curvature over the Brillouin zone.

$$\Omega(\mathbf{k}) = \sum_n f_n \Omega_n(\mathbf{k}),$$
$$\Omega_n(\mathbf{k}) = -\sum_{n' \neq n} 2\mathrm{Im} \frac{\langle \psi_{n\mathbf{k}} | v_x | \psi_{n'\mathbf{k}} \rangle \langle \psi_{n'\mathbf{k}} | v_y | \psi_{n\mathbf{k}} \rangle}{(\varepsilon_{n'\boldsymbol{k}} - \varepsilon_{n\boldsymbol{k}})^2}, \quad (1)$$

where n is the band index, f_n the Fermi-Dirac distribution function, $\psi_{n\boldsymbol{k}}$ and $\varepsilon_{n\boldsymbol{k}}$ are the Bloch wave-function and energy of the n-th band at $\boldsymbol{k}$ point, respectively. And $v_{x/y}$ is the velocity operator. Here we used the maximally-localized Wannier functions to calculate the Berry curvature as provided by the WANNIER90 package[46].

1. Hasan, M. Z. & Kane, C. L. Colloquium: Topological insulators. *Rev. Mod. Phys.* **82**, 3045–3067 (2010).
2. Qi, X.-L. & Zhang, S.-C. Topological insulators and superconductors. *Rev. Mod. Phys.* **83**, 1057–1110 (2011).
3. Bernevig, B. A., Hughes, T. L. & Zhang, S.-C. Quantum Spin Hall Effect and Topological Phase Transition in HgTe Quantum Wells. *Science* **314**, 1757–1761 (2006).
4. König, M. *et al.* Quantum Spin Hall Insulator State in HgTe Quantum Wells. *Science* **318**, 766–770 (2007).
5. Fu, L., Kane, C. L. & Mele, E. J. Topological Insulators in Three Dimensions. *Phys. Rev. Lett.* **98**, 106803 (2007).
6. Zhang, H. *et al.* Topological insulators in Bi_2Se_3, Bi_2Te_3 and Sb_2Te_3 with a single Dirac cone on the surface. *Nat. Phys.* **5**, 438–442 (2009).
7. Chen, Y. L. *et al.* Experimental Realization of a Three-Dimensional Topological Insulator, Bi_2Te_3. *Science* **325**, 178–181 (2009).
8. Fu, L. & Kane, C. L. Topological insulators with inversion symmetry. *Phys. Rev. B.* **76**, 045302 (2007).
9. Soluyanov, A. A. & Vanderbilt, D. Computing topological invariants without inversion symmetry. *Phys. Rev. B.* **83**, 235401 (2011).
10. Kane, C. L. & Mele, E. J. Quantum Spin Hall Effect in Graphene. *Phys. Rev. Lett.* **95**, 226801 (2005).
11. Kane, C. L. & Mele, E. J. Z_2 topological order and the quantum spin Hall effect. *Phys. Rev. Lett.* **95**, 146802 (2005).
12. Min, H. *et al.* Intrinsic and Rashba spin-orbit interactions in graphene sheets. *Phys. Rev. B.* **74**, 165310 (2006).
13. Yao, Y. *et al.* Spin-orbit gap of graphene: First-principles calculations. *Phys. Rev. B.* **75**, 041401 (2007).
14. Boettger, J. C. & Trickey, S. B. First-principles calculation of the spin-orbit splitting in graphene. *Phys. Rev. B.* **75**, 121402 (2007).
15. Gmitra, M. *et al.* Band-structure topologies of graphene: Spin-orbit coupling effects from first principles. *Phys. Rev. B.* **80**, 235431 (2009).
16. Castro Neto, A. H. & Guinea, F. Impurity-Induced Spin-Orbit Coupling in Graphene. *Phys. Rev. Lett.* **103**, 026804 (2009).
17. Weeks, C. *et al.* Engineering a Robust Quantum Spin Hall State in Graphene via Adatom Deposition. *Phys. Rev. X.* **1**, 021001 (2011).
18. Jin, K. H. & Jhi, S. H. Proximity-induced giant spin-orbit interaction in epitaxial graphene on a topological insulator. *Phys. Rev. B.* **87**, 075442 (2013).
19. Liu, Z. *et al.* Stable Nontrivial Z_2 Topology in Ultrathin Bi (111) Films: A First-Principles Study. *Phys. Rev. Lett.* **107**, 136805 (2011).
20. Murakami, S. Quantum Spin Hall Effect and Enhanced Magnetic Response by Spin-Orbit Coupling. *Phys. Rev. Lett.* **97**, 236805 (2006).
21. Wada, M., Murakami, S., Freimuth, F. & Bihlmayer, G. Localized edge states in two-dimensional topological insulators: Ultrathin Bi films. *Phys. Rev. B.* **83**, 121310 (2011).
22. Hirahara, T. *et al.* Interfacing 2D and 3D Topological Insulators: Bi(111) Bilayer on Bi_2Te_3. *Phys. Rev. Lett.* **107**, 166801 (2011).
23. Yang, F. *et al.* Spatial and Energy Distribution of Topological Edge States in Single Bi(111) Bilayer. *Phys. Rev. Lett.* **109**, 016801 (2012).
24. Kim, S. H. *et al.* Edge and interfacial states in a two-dimensional topological insulator: Bi(111) bilayer on Bi_2Te_2Se. *Phys. Rev. B.* **89**, 155436 (2014).
25. Onoda, M. & Nagaosa, N. Quantized Anomalous Hall Effect in Two-Dimensional Ferromagnets: Quantum Hall Effect in Metals. *Phys. Rev. Lett.* **90**, 206601 (2003).
26. Qi, X.-L., Wu, Y.-S. & Zhang, S.-C. Topological quantization of the spin Hall effect in two-dimensional paramagnetic semiconductors. *Phys. Rev. B.* **74**, 085308 (2006).
27. Liu, C.-X. *et al.* Quantum Anomalous Hall Effect in $Hg_{1-y}Mn_yTe$ Quantum Wells. *Phys. Rev. Lett.* **101**, 146802 (2008).
28. Qiao, Z. *et al.* Quantum anomalous Hall effect in graphene from Rashba and exchange effects. *Phys. Rev. B.* **82**, 161414 (2010).
29. Ezawa, M. Valley-Polarized Metals and Quantum Anomalous Hall Effect in Silicene. *Phys. Rev. Lett.* **109**, 055502 (2012).
30. Yu, R. *et al.* Quantized Anomalous Hall Effect in Magnetic Topological Insulators. *Science* **329**, 61–64 (2010).
31. Sofo, J. O., Chaudhari, A. S. & Barber, G. D. Graphane: A two-dimensional hydrocarbon. *Phys. Rev. B.* **75**, 153401 (2007).
32. Elias, D. C. *et al.* Control of Graphene's Properties by Reversible Hydrogenation: Evidence for Graphane. *Science* **323**, 610–613 (2009).
33. Xu, Y. *et al.* Large-Gap Quantum Spin Hall Insulators in Tin Films. *Phys. Rev. Lett.* **111**, 136804 (2013).
34. Miura, Y. *et al.* First principles studies for the dissociative adsorption of H_2 on graphene. *J. Appl. Phys.* **93**, 3395–3400 (2003).
35. Ao, Z. M. & Peeters, F. M. Electric field: A catalyst for hydrogenation of graphene. *Appl. Phys. Lett.* **96**, 253106 (2010).
36. Wittel, K. & Manne, R. Atomic spin-orbit interaction parameters from spectral data for 19 elements. *Theor. Chim. Acta.* **33**, 347–349 (1974).
37. Song, Z. *et al.* Quantum Spin Hall Insulators of BiX/SbX (X = H, F, Cl, and Br) Monolayers with a Record Bulk Band Gap. arXiv:14022399 (2014).
38. Wang, Z. F., Chen, L. & Liu, F. Tuning Topological Edge States of Bi(111) Bilayer Film by Edge Adsorption. *Nano. Letters.* **14**, 2879–2883 (2014).
39. Jin, K. H. & Jhi, S. H. Effect of atomic impurities on the helical surface states of the topological insulator Bi_2Te_3. *J. Phys. Condens. Matt.* **24**, 175001 (2012).
40. Chang, C.-Z. *et al.* Experimental Observation of the Quantum Anomalous Hall Effect in a Magnetic Topological Insulator. *Science* **340**, 167–170 (2013).
41. Blöchl, P. E. Projector augmented-wave method. *Phys. Rev. B.* **50**, 17953–17979 (1994).
42. Kresse, G. & Joubert, D. From ultrasoft pseudopotentials to the projector augmented-wave method. *Phys. Rev. B.* **59**, 1758–1775 (1999).
43. Perdew, J. P., Burke, K. & Ernzerhof, M. Generalized Gradient Approximation Made Simple. *Phys. Rev. Lett.* **77**, 3865–3868 (1996).

44. Thouless, D. J., Kohmoto, M., Nightingale, M. P. & den Nijs, M. Quantized Hall Conductance in a Two-Dimensional Periodic Potential. *Phys. Rev. Lett.* **49**, 405–408 (1982).
45. Yao, Y. *et al*. First Principles Calculation of Anomalous Hall Conductivity in Ferromagnetic bcc Fe. *Phys. Rev. Lett.* **92**, 037204 (2004).
46. Mostofi, A. A. *et al*. wannier90: A tool for obtaining maximally-localised Wannier functions. *Comput. Phys. Commun.* **178**, 685–699 (2008).

Acknowledgments

This works was supported by Institute for Basic Science (IBS) through the Center for Artificial Low Dimensional Electronic Systems and the SRC Center for Topological Matter (2011-0030789). The authors would like to acknowledge the support from KISTI supercomputing center through the strategic support program for supercomputing application research (No. KSC-2012-C3-37).

Author contributions

K.-H.J. performed the calculation and analysis and wrote the manuscript. S.-H.J. directed the work, contributed to the analysis and the manuscript writing.

Additional information

Supplementary information accompanies this paper at http://www.nature.com/scientificreports

Competing financial interests: The authors declare no competing financial interests.

How to cite this article: Jin, K.-H. & Jhi, S.-H. Quantum anomalous Hall and quantum spin-Hall phases in flattened Bi and Sb bilayers. *Sci. Rep.* **5**, 8426; DOI:10.1038/srep08426 (2015).